

Hi-C 2.1 Observations of Small-Scale Miniature-Filament-Eruption-Like Cool Ejections in Active Region Plage

ALPHONSE C. STERLING,¹ RONALD L. MOORE,^{1,2} NAVDEEP K. PANESAR,^{1,3,4} KEVIN P. REARDON,⁵ MOMCHIL MOLNAR,^{5,6}
LAUREL A. RACHMELER,¹ SABRINA L. SAVAGE,¹ AND AMY R. WINEBARGER¹

¹*NASA/Marshall Space Flight Center, Huntsville, AL 35812, USA*

²*Center for Space Plasma and Aeronomic Research,*

University of Alabama in Huntsville, Huntsville, AL 35899, USA

³*Bay Area Environmental Research Institute, NASA Research Park, Moffett Field, CA 94035, USA*

⁴*Lockheed Martin Solar and Astrophysics Laboratory, Palo Alto, CA 94304, USA*

⁵*National Solar Observatory, Boulder, CO 80303, USA*

⁶*Department of Astrophysics and Planetary Sciences, University of Colorado, Boulder, CO, 80303, USA*

ABSTRACT

We examine 172 Å ultra-high-resolution images of a solar plage region from the Hi-C 2.1 (“Hi-C”) rocket flight of 2018 May 29. Over its five-minute flight, Hi-C resolves a plethora of small-scale dynamic features that appear near noise level in concurrent Solar Dynamics Observatory (SDO) Atmospheric Imaging Assembly (AIA) 171 Å images. For ten selected events, comparisons with AIA images at other wavelengths and with the Interface Region Imaging Spectrograph (*IRIS*) images indicate that these features are cool (compared to the corona) ejections. Combining Hi-C 172 Å, AIA 171 Å, *IRIS* 1400 Å, and H α , we see that these ten cool ejections are similar to the H α “dynamic fibrils” and Ca II “anemone jets” found in earlier studies. The front of some of our cool ejections are likely heated, showing emission in *IRIS* 1400 Å. On average, these cool ejections have approximate widths: $3''.2 \pm 2''.1$, (projected) maximum heights and velocities: $4''.3 \pm 2''.5$ and 23 ± 6 km s⁻¹, and lifetimes: 6.5 ± 2.4 min. We consider whether these Hi-C features might result from eruptions of sub-minifilaments (smaller than the minifilaments that erupt to produce coronal jets). Comparisons with SDO’s Helioseismic and Magnetic Imager (HMI) magnetograms do not show magnetic mixed-polarity neutral lines at these events’ bases, as would be expected for true scaled-down versions of solar filaments/minifilaments. But the features’ bases are all close to single-polarity strong-flux-edge locations, suggesting possible local opposite-polarity flux unresolved by HMI. Or, it may be that our Hi-C ejections instead operate via the shock-wave mechanism that is suggested to drive dynamic fibrils and the so-called type I spicules.

Keywords: Sun: filaments, prominences — Sun: corona — Sun: magnetic fields — Sun: UV radiation — Sun: faculae, plages — Sun: transition region

1. INTRODUCTION

Observations of plage regions of the Sun in EUV at 171 Å with the Solar Dynamics Observatory (SDO) Atmospheric and Imaging Assembly (AIA) hint at unresolved omnipresent dynamic activity of size scale of ~ 1 –few arcseconds, varying on times scales near that channel’s 12-s cadence. Here we report on observations of resolved views of these features from the 5-minute suborbital rocket flight of the High-Resolution Coronal Imager, version 2.1 (Hi-C 2.1; hereafter, “Hi-C”), observing at 172 Å.

Similar small-scale plage features have been observed at high resolution in H α (Berger et al. 1999; De Pontieu et al. 1999), where they and similar features have been called various names, including “dynamic fibrils” (e.g. De Pontieu et al. 2007a) and “type-1 spicules” (De Pontieu et al. 2007b). It is thought that many such H α features result from wave oscillations that evolve into shocks in the chromosphere (e.g., Hansteen et al. 2006; De Pontieu et al. 2007a). They

are also similar to Ca II chromospheric “anemone jets” (Shibata et al. 2007), which are suggested to result from reconnection between an emerging bipole (or any bipole) and ambient field (e.g., Shibata et al. 2007; Takasao et al. 2013).

Meanwhile, other recent studies have shown that solar coronal jets frequently result from eruption of small-scale filaments (*minifilaments*), that are apparent in AIA EUV channels, including 171 Å, of sizes ranging over $\sim 11''$ – $24''$ (Sterling et al. 2015; Panesar et al. 2016), and the production of jets from minifilament eruptions has been modeled (Wyper et al. 2017). Here, we will consider whether the events we resolve in Hi-C are cool ejections into the very low corona result from even-smaller-scale versions of such minifilament eruptions (which here we will call “sub-minifilament eruptions”).

2. DATA SET

Hi-C flew on a sounding rocket on 2018 May 29, observing the Sun in 172 Å Fe IX/X emission for about 5 minutes, with usable data from 18:56:26–19:01:43 UT (Rachmeler et al. 2019). Its field of view (FOV) covered active region NOAA AR 12712. Here we examine a $40'' \times 40''$ subregion in the plage of the AR, containing only plage and a small sunspot (Figure 1(a–b)). Hi-C has $\sim 0''.1$ pixels, and 4.4-s cadence (Rachmeler et al. 2019). Here we used movies with occasional jumps in cadence because we avoid images most strongly blurred by rocket jitter; the video accompanying Figure 1(c) shows that the resolution varied somewhat over the time period as a result. Nonetheless, we were able to follow the progress of several of the cool ejections, and we focus on ten of them here.

In addition to Hi-C, we examined all seven AIA EUV channels of this subregion (Lemen et al. 2012). As we will show, we could identify our ten Hi-C cool ejections in AIA 171 Å. Otherwise however, the only AIA channels where we see counterparts to our Hi-C features are 304 Å, 193 Å, and weakly in 211 Å, which are the AIA EUV channels with the coolest peak temperature response (respectively peaking at $\sim 5 \times 10^4$ and 1.5×10^6 K), in addition to 171 Å ($\sim 6 \times 10^5$ K). (Thus, in the context of this paper, by *cool ejections* we mean features that appear primarily in absorption in 172 Å and 171 Å images, with little or no signal in hotter channels.) The AIA images have $0''.6$ pixels and 12-s cadence. We also examine slit-jaw images from the Interface Region Imaging Spectrograph (IRIS) (De Pontieu et al. 2014) taken with $0''.17 \times 2$ (double-binned) pixels at ~ 13 s cadence in four filters: 1330 Å (C II, 30,000 K) and 1400 Å (Si IV, 65,000 K), each with a 40 Å bandpass; and 2796 Å (Mg II k, 15,000 K) and 2831 Å (Mg II h/k wing, 6000 K), each with a 4 Å bandpass. Additionally, we use line-of-sight magnetograms from the SDO Helioseismic and Magnetic Imager (HMI), which has $0''.5$ pixels and 45 s cadence (Scherrer et al. 2012). See §4 for information on preliminary H α observations.

3. OBSERVATIONS AND RESULTS

Our selected FOV is full of fine-scale dynamic structure (see Figure 1(c) video). In Figure 1(c), arrows show our ten selected features (Table 1), and boxes show their footpoints (i.e. where they appear to lift off the surface in Hi-C or AIA 171 videos).

We define the cool-ejection lifetimes (Table 1), as the time from the feature’s first clear upward motion, until either it returned to the surface or faded. (Strictly speaking, the motion we observe is in the plane normal to our LOS. Throughout this paper we assume that the actual motion is along the magnetic field extending from the surface into the corona, giving the features a basic up- and down-component to their motion, such as for spicules.) This duration frequently exceeded the 5-minute Hi-C flight. Hence we supplemented our observations with movies made from AIA 171 Å images, that extended several minutes before and after the Hi-C time window (Figure 1(d) and accompanying video). For each event, we were able to identify the Hi-C features in AIA, albeit at substantially reduced resolution. We used an early (pre-public-release) version of the Hi-C images that required small manual shifts for alignment with the AIA images, and that had residual jitter resulting in jumps of order one-half arcsecond over the video’s duration. We estimate our final AIA-Hi-C alignment to be accurate to $\lesssim 1''$ over our selected FOV.

3.1. Hi-C 172 Å Morphology

From extensive relatively recent investigations, prevailing views for the explanation of many chromospheric dynamic features in plage is that they are shock driven, or that they are driven by reconnection between emerging flux and ambient field; these ideas are discussed at length in references of §1, and we also consider these ideas further in §4. Here we consider whether the features we observe here, features that are prominent in Hi-C images, might be smaller cousins of the minifilament eruptions that drive coronal jets. Because we now know that many jets are driven by eruptions of small-scale filaments, we consider it natural to entertain the possibility that the smaller jets we observe

here might be driven by even smaller-scale eruptions; that is, we consider whether they might be sub-minifilament eruptions. In this Section we discuss the morphology of the features mainly in this context. We first highlight two better-observed events: 3 and 9.

Event 3 begins near 18:58:27 UT (Figures 1(c,e) videos) and evolves into an upward-moving prominent dark feature ($\sim 18:59:28$ UT). It has an obvious compact, circular shape, but there may also be dark extensions of this feature to the southeast. Subsequently, the prominent dark feature rises with a (projected) velocity of $\sim 20 \text{ km s}^{-1}$, and starts to bend into a curved path near the end of the Hi-C video ($\sim 19:01:26$ UT). Its subsequent evolution is visible but harder to track in AIA 171 Å, and by 19:04:57 UT it has faded and is no longer identifiable.

Event 9 has a somewhat different character. It unambiguously begins as a bright, long and thin filament-like feature that rises upward from its western end ($\sim 18:56:56$ UT; Figures 1(c,f) videos). A dark component appears adjacent to the brighter feature, eventually reaching (apparently) higher than and beyond the brighter feature ($\gtrsim 18:59:28$ UT). That dark feature may eventually also follow a curved trajectory near the end of the Hi-C video ($\gtrsim 19:00:29$ UT). Continuing in AIA 171, the feature falls and fades away by 19:06:45 UT.

It is plausible that event 3 is a more-compact version of event 9, with both being sub-minifilament eruptions. In support of this interpretation, event 3 is also similar to the compact roughly-circular “blob” feature that produced a jet in Adams et al. (2014). In particular, Figure 6(c) of that paper shows the circular dark structure surrounded by brightenings in 171 Å. Considering other evidence (e.g. Shen et al. 2012; Sterling et al. 2015; Panesar et al. 2016, 2018a), it is now almost certain that the jet-producing blob of Adams et al. (2014) was an erupting minifilament. Hence, even though the dark feature of event 3 is too amorphous to identify unambiguously as an erupting sub-minifilament, the additional jet studies suggest that it plausibly could be. Thus, the event-3 ejection may be a sub-minifilament eruption. For event 9, its early brightenings could result from reconnections between the magnetic field enveloping the erupting filament-like feature with surrounding field, resulting in a cocoon of brighter emission (e.g., Sterling et al. 2011; Li & Ding 2017).

We next consider the remaining eight events.

Event-1’s rise is visible in Hi-C, while its decay is only seen in AIA and hence is less clear. This feature rises in-sync with event 3, and their bases (boxes in Figure 1(c)) nearly overlap; thus the two events could be part of the same magnetic structure, although we cannot identify a definitive connection. Event 1 appears to be an upward-rising loop or (sub-mini)filament structure. For example, at 19:00:29 UT, it appears as an absorbing feature $\sim 5''$ long and $\sim 2''$ tall. By 19:01:30 UT it has darkened, and the east side appears as a very short $\sim 3''$ -long jet structure.

Event 2 seems similar to event 9: it is an elongated emission feature, extending from the arrow head to the edge of the FOV in the video accompanying Figure 1(c) at 18:57:53 UT. From 18:59:28 UT and until the end of the Hi-C movie, a portion of this feature ejects outward, north-northeastward, as a narrow ($\sim 1''$) jet in emission. This is similar to some narrow-spire coronal jets, whereby a minifilament can erupt upward into the base region of the jet, with jet material flowing out along a narrow spire (good examples are events 6 and 8 of Sterling et al. 2015). Therefore event 2 (and also likely event 9, and similar events) is a candidate for being a small-scale version of the minifilament eruptions that produce a coronal jet.

Event 4 is not fully resolved, but includes a weakly-emitting component moving westward over 18:59:02–18:59:33 UT, followed by an upward rise of a curtain of absorbing material, which remains elevated at the end of the Hi-C movie and is about $5''$ wide and $2''.5$ high at its tallest. This plausibly resembles a very weak failed/confined (sub-mini)filament eruption.

Event 5 is a surge-like ejection that is larger than those so-far examined, and consequently (with insight from Hi-C) clearly identifiable in AIA 171. Hi-C only captures its return to the surface, but clearly shows a brighter portion at the feature’s top. From about 18:51:57 UT, AIA shows a bright feature leading the rise onset, similar to the initial brightenings in events 2 and 9.

Event 6, as also Event 5, is falling as the Hi-C movie starts (its apparent rise being clearly visible in pre-Hi-C AIA images). During the first 30 s of Hi-C it seems to be part of Event 7, but by 18:57:22 UT, it has faded while Event 7 has not; this, along with its earlier behavior over 18:53–18:55 UT in AIA 171, makes this event appear to be distinct from event 7. Again, there is a bright upper edge of the feature, clear in Hi-C (e.g. 18:56:34 UT). From the start of the Hi-C movie until 18:57:00 UT, this event’s absorbing portion appears to have a large horizontal extent ($\sim 5''$), similar to event 1.

Event 7 also begins prior to Hi-C observations. Over about 18:50–18:53 UT, AIA shows an emission feature moving upward in sync with the absorption material. In this case, Hi-C shows the absorption feature to have more of a long-narrow morphology (appearing as a small surge or spicule) than does event 6.

Event 8 roughly moves in sync with event 9, and their bases nearly overlap; so similar to the event 1 and 3 pair, these two features also may be part of the same magnetic structure (e.g., both may be in separate small, low-lying, adjacent bipoles, that reside beneath the same overlying magnetic enveloping field; eruption of one could trigger eruption of the second). Regarding them as separate events, event 8 is similar to event 1 in that it has a larger horizontal extent than vertical rise, and so as with event 1 it may be a confined eruption of a sub-minifilament structure.

Event 10 shows a clear bright front portion to an uprising absorption column, moving toward the northeast and forming a long and narrow ejection. AIA indicates that the feature reaches its maximum extent at about when the Hi-C movie ends.

3.2. AIA and IRIS Morphology

We examined other AIA EUV channels for indications of the ten features. Among these, hints of the features were present in the “cooler” AIA channels, 193 Å and 211 Å, while they were not visible in hotter channels such as 94 Å and 131 Å. AIA 304 Å shows well event 5, which in Hi-C is the largest and darkest of the absorbing features. Also the emission components of events 2 and 9 are weakly discernible in 304 as they erupt away from the surface. None of the remaining seven features are unambiguously discernible from myriad surrounding and background not-fully-resolved dynamical motions in the 304 Å movies.

We manually aligned *IRIS* images with features in AIA and HMI. Although *IRIS* 1400 shows little obvious overlap with the bodies of our ten Hi-C events, close inspection reveals that tops of at least events 5, 9, and 10 are obvious in 1400 emission (Figure 3). In some cases, such as event 5, the 1400 emission is bright during the event’s extension phase, but later (after 18:53:55 UT) the feature faded in 1400 even though it was still bright in Hi-C. Matches of other events in 1400 were less obvious (perhaps due to a smaller projection angle). *IRIS* 1330 shows similar morphology for events 5, 9, and 10, while corresponding features were difficult-to-detect or non-existent in the two remaining (cooler) *IRIS* channels.

Overall, these findings support that some components of our features are heated to transition-region temperatures.

3.3. Magnetic Setting

We confirmed that the default HMI magnetogram alignment with AIA was accurate through comparisons with various features, including the sunspots in the full Hi-C FOV.

Figure 2(a) shows the magnetogram with contours, and Figure 2(b) shows the same contours on the Figure 1(c) Hi-C 172 Å image. Most apparent from the Hi-C overlay is that the plage appears unipolar, the magnetogram showing only negative polarity. It is also however immediately apparent that the negative-polarity strength is highly nonuniform, with stronger and weaker locations of negative field throughout the plage region. Therefore, while we see that all of our ten cool ejections originate from a single-polarity location in HMI, we also see that all of them are within a couple arcseconds or so (about the reliability of the overlay alignment) of an “edge” between stronger and weaker negative field. We will return to this point in the Discussion.

4. SUMMARY AND DISCUSSION

A preliminary comparison with H α line-core intensity images of resolution comparable to Hi-C (but with highly varying seeing quality) obtained from the Dunn Solar Telescope at Sacramento Peak Solar Observatory, supplied by two of us (KPR and MM), shows that our Hi-C features do have H α components. These H α features are nearly co-spatial with what we see with Hi-C, and display similar dynamics. Thus our observed features plausibly make up some part of the population of small-scale dynamic fibrils observed in H α and in EUV. Also however, it is likely that they also coincide with some part of the population of anemone jets observed in Ca II (cf. Morita et al. 2010). Properties for the two features are very similar; e.g., for chromospheric anemone jets, Shibata et al. (2007) give lengths of $\sim 3''$ – $7''$, and velocities 10–20 km/s, which are very close to the Table 1 values for the Hi-C features ($\sim 2''$ – $7''$ and 10–20 km/s, respectively). The Hi-C features width ($1''$ – $5''$) are larger than those of the Shibata et al. (2007) anemone jets ($0''.2$ – $0''.4$), which might be a consequence of the respective observed wavelengths.

Various studies suggest that many of the dynamic fibrils are driven by acoustic waves that steepen into shocks in the chromosphere (e.g., De Pontieu et al. 2004; Hansteen et al. 2006; De Pontieu et al. 2007a,b), resulting in oscillating

and repeated dynamic fibrils at close to the acoustic cutoff period, as in the rebound shocks of [Hollweg \(1982\)](#) (modified by radiation effects, e.g. [Sterling & Mariska 1990](#)). When the magnetic flux tube on which the field-aligned oscillations occur is sufficiently inclined to the vertical, observations and numerical simulations support that the local acoustic cutoff period for acoustic waves along the flux tube is long enough to permit enhanced excitement of waves (and hence shocks, and dynamic fibrils) along the tube at the photospheric p -mode oscillation period ([Suematsu 1990](#); [De Pontieu et al. 2007b](#); [Martínez-Sykora et al. 2009](#); [Heggland et al. 2011](#)).

Even if many dynamic fibrils are driven by shocks, some other dynamic features originating in the chromosphere could be due to a different mechanism, such as magnetic reconnection; this might not be surprising, but would require a mixture of magnetic polarities in place. There is substantial work indicating that many spicules *outside of plages* are driven by a reconnection mechanism; these features have been called “type II spicules” ([De Pontieu et al. 2007b](#); [Pereira, De Pontieu, & Carlsson 2012](#); [Martínez-Sykora et al. 2017](#)). Some portion of at least those non-plage small-scale dynamic events might fall on a continuum of reconnection-driven spicule-sized features, macrospicules, and various surges and jets (e.g., [Canfield et al. 1996](#); [Chae et al. 1998](#); [Hansteen et al. 2006](#); [De Pontieu et al. 2007a](#); [Roupe van der Voot et al. 2007](#); [Shibata et al. 2007](#); [De Pontieu et al. 2007a](#); [Sterling & Moore 2016](#)).

On the other hand, various different studies suggest that the anemone jets result from emerging flux reconnecting with ambient field (e.g., [Shibata et al. 2007](#); [Nishizuka et al. 2008](#); [Morita et al. 2010](#); [Nishizuka et al. 2011](#); [Singh et al. 2012](#)). These jets have an “inverted-Y” shape at their base, which is consistent with the emerging flux model for jets (or any jet model based on reconnection between a bipole and ambient field) ([Shibata et al. 1994](#); [Yokoyama & Shibata 1995](#); [Moreno-Insertis et al. 2008](#)). Because our observed Hi-C features resemble anemone jets, it is possible that undetected emerging flux is the driver of our Hi-C events.

Regarding coronal jets, especially in coronal holes and quiet Sun, there exist strong observational evidence that often the jets result from minifilament/flux rope eruptions, where the minifilament/flux ropes are built and triggered to erupt by magnetic flux cancellation (e.g. [Shen et al. 2012](#); [Young & Muglach 2014a](#); [Sterling et al. 2015](#); [Panesar et al. 2016, 2018a](#); [McGlasson et al. 2019](#)). In some cases however the minifilament/flux rope might be triggered to erupt by a different process (e.g., [Kumar et al. 2019](#)). And we cannot rule out the possibility that some jets might result from the flux-emergence process in the absence of clear flux cancellation.

Because many coronal jets result from flux-cancellation-built-and-triggered minifilament eruptions, in this work we are asking whether the smaller-than-jet cool ejections that we observe *in plage*, being prominent in Hi-C 172 images, might be driven by eruptions of smaller-scale filament-like features that are smaller than the minifilaments that erupt to drive coronal jets; we have focused on this viewpoint in this paper. Perhaps the most glaring lack of evidence for the erupting (mini)filament idea however is that (mini)filaments always occur at the inversion line of mixed-polarity locations (e.g., for jet minifilaments see [Panesar et al. 2016, 2018a](#)). Another obvious lack is that there is no definitive bright point at the base of our cool ejections corresponding to the jet bright point (JBP) often appearing at jet bases ([Shibata et al. 1992](#); [Sterling et al. 2015](#)).

Nonetheless, because of the non-uniform nature of the (seemingly) unipolar field of the plage region (Figure 2), it is possible that weak, small-scale opposite-polarity intrusions exist in the plage. In Figure 2, these would take the form of positive-polarity elements too small/weak to be detected with HMI, but that could result in localities in the HMI magnetogram having weaker negative-field strength than in the surrounding plage. Since our ten cool ejections are all rooted within a short distance of a field-intensity edge (Figure 2), it is possible that small-scale positive-polarity elements might exist in those regions and give rise to the features we observe, as that flux cancels with surrounding dominant (negative) polarity. Similarly, brightenings corresponding to JBPs could exist but be very weak and subtle or hidden, as the magnetic reconnection that would be expected to be the source of those brightenings would occur in a denser region of the atmosphere than in the coronal jet case, with radiative losses from the dense material robbing much of the energy that would otherwise appear as a brightening ([Sterling & Moore 2016](#) discuss a similar situation regarding weak brightenings, and [Panesar et al. 2018b](#) discuss similar small-scale flux patches and brightenings).

We briefly consider our events in terms of the still-speculative suggestion of [Sterling & Moore \(2016\)](#) that eruptions of filament(-like) sheared/twisted magnetic-field structures of size scales of filaments, minifilaments, and so-far-unseen microfilaments might respectively drive CMEs, coronal jets, and many spicules. This is consistent with suggestions of [Moore et al. \(1977\)](#), [Moore \(1990\)](#), and [Shibata \(1999\)](#). Plotting the number on the Sun at a given time of each category of erupting feature against its size shows an approximate power law (Figure 2 of [Sterling & Moore 2016](#)). We can add a point to this plot with our cool ejections: simply extrapolating ten events over the $40'' \times 40''$ Figure 1(c) FOV to the entire solar surface implies an upper bound of $\sim 70,000$ cool events ($\pm 50\%$ as an uncertainty estimate)

occurring on the Sun at any point in time. These values, with the average width in Table 1 of $\sim 2300 \pm 1500$ km, gives the red point in Figure 4. Our new point is offset above the original power-law curve, but not totally inconsistent with it considering the crudeness of the estimates. The offset might also suggest a higher proportion of such events in plages, compared to the non-plage spicule and jet estimates of [Sterling & Moore \(2016\)](#). We add two caveats: first, because usually only a small fraction of the Sun, $\sim 10\%$, is covered by plage and magnetic network flux, our estimate of the number events on the Sun could be a factor of ten too high, and thus we extend a dashed line on the plot down to that reduced value. Second, the number of spicules might be higher than shown here ($\sim 2 \times 10^7$, according to [Judge & Carlsson 2010](#)).

We do emphasize however that it has not been established observationally how spicules are driven. In addition to the ideas cited above, other possibilities discussed include Alfvén waves (e.g., [Hollweg et al. 1982](#); [Kudoh & Shibata 1999](#); [Matsumoto & Shibata 2010](#); [Cranmer & Woolsey 2015](#); [Iijima & Yokoyama 2017](#); [Martínez-Sykora et al. 2017](#)), or that spicules are sheet-like magnetic structures ([Judge et al. 2012](#)). Moreover, the question of whether there are two types of spicules, type I and type II as defined in [De Pontieu et al. \(2007b\)](#), is still unresolved; see [Zhang et al. \(2012\)](#) and [Pereira, De Pontieu, & Carlsson \(2012\)](#) for opposing viewpoints; also see [Anan et al. \(2010\)](#). Also, the relationship between the pre-*Hinode*-era “classical” spicules of, e.g., [Beckers \(1972\)](#), and these possible spicules types is still being sorted out ([Sterling et al. 2010](#); [Pereira et al. 2013](#)). More recent spicule reviews than [Beckers \(1972\)](#) include [Sterling \(2000\)](#) and [Tsiropoula et al. \(2012\)](#).

We find that our Hi-C features show strong similarities to the dynamic fibrils referred to as “type-I spicules” ([De Pontieu et al. 2004, 2007b](#)); the average lifetimes (6.4 min, from Hi-C and AIA combined observations) and upward velocities (23 km s^{-1}) from our features from Table 1 match well with the type I parameters (3–7 min, and $< 40 \text{ km s}^{-1}$). The shocks suggested as being the drivers of dynamic fibrils are an alternative to our Hi-C events being small versions of coronal jets. The jets often result from magnetic-flux cancelations forming minifilaments ([Panesar et al. 2017](#)) that are triggered to erupt by further cancelation ([Panesar et al. 2016, 2018a](#); [Sterling et al. 2017](#)), producing the jets ([Sterling et al. 2015](#)). If however there are small-scale mixed-polarity elements embedded inside of the seemingly-unipolar plage field, then another possibility is that the sloshing from granular motions and photospheric *p*-mode oscillations could drive cancelation among small-scale elements, generating the Hi-C features (and perhaps type I spicules) in a manner similar to how coronal jets are produced (compare [Morton et al. 2012](#)).

More generally, because we do not observe clear evidence for mixed polarity, converging flux, or emerging flux, at this time we cannot rule out any of a variety of other mechanisms for driving the small-scale Hi-C features, including various ideas for jets (e.g., [Shibata & Uchida 1986](#); [Yokoyama & Shibata 1995](#); [Pariat et al. 2009](#)), or any of the various models for spicules. Alternatively, the ejections could be a kind of plasmoid (or flux rope in 3D space) (e.g. [Bhattacharjee et al. 2009](#); [Ji & Daughton 2011](#)).

Long-term detailed studies (preferably satellite based) with a high-resolution EUV instrument similar to Hi-C, combined with high-resolution chromospheric images and photospheric/chromospheric magnetograms, e.g. from CRISP, CHROMIS, BBSO, and the upcoming DKIST facility, and with state-of-the-art numerical simulations, will help determine whether the features we observe here are due to chromospheric shocks, jet-like minifilament eruptions, or some other mechanism. A direct near-future test will be with the high-resolution magnetograms from DKIST, which should tell whether small-scale mixed-polarity elements exist within strong plage, and whether those elements undergo cancelation at locations near where cool ejections originate.

We thank B. De Pontieu for very fruitful discussions, and an anonymous referee for a very detailed and helpful report. A.C.S. and R.L.M. received funding from the Heliophysics Division of NASA’s Science Mission Directorate through the Heliophysics Guest Investigators (HGI) Program, and the *Hinode* Project. N.K.P.’s is supported by NASA SDO/AIA funding (NNG04EA00C); and previously by the NASA Postdoctoral Program at NASA/MSFC, administered by Universities Space Research Association under contract with NASA. We acknowledge the Hi-C 2.1 instrument team for making the second re-flight data available under the NASA Heliophysics Technology and Instrument Development for Science (HTIDS) Low Cost Access to Space (LCAS) program. MSFC/NASA led the mission with partners including the Smithsonian Astrophysical Observatory, the University of Central Lancashire, and Lockheed Martin Solar and Astrophysics Laboratory. *IRIS* is a NASA small explorer mission developed and operated by LMSAL with mission

operations executed at NASA Ames Research center and major contributions to downlink communications funded by ESA and the Norwegian Space Centre.

REFERENCES

- Adams, M., Sterling, A. C., Moore, R. L., & Gary, G. A. 2014, *ApJ*, 783, 11
- Anan, T., Kitai, R., Kawate, T., et al. 2010, *PASJ*, 62, 871
- Beckers, J. M. 1972, *ARA&A*, 10, 73
- Berger, T. E., De Pontieu, B., Schrijver, C. J., & Title, A. M. 1999, *ApJL*, 519, L97
- Bhattacharjee, A., Huang, Yi-Min, Yang, H., & Rogers, B. 2009, *PhPl*, 16, 2102
- Canfield, C. C., Reardon, K. P., Leka, K. D., Shibata, K., Yokoyama, T., & Shimojo, M. 1996, *ApJ*, 464, 1016
- Chae, J., Wang, H., Lee, C.-Y., & Goode, P. R. 1998, *ApJL*, 504, L123
- Cranmer, S. R., & Woolsey, L. N. 2015, *ApJ*, 812, 71
- De Pontieu, B., Berger, T. E., Schrijver, C. J., & Title, A. M. 1999, *SoPh*, 190, 419
- De Pontieu, B., Erdélyi, R., & James, S. P. 2004, *Nature*, 430, 536
- De Pontieu, B., Hanstten, V. H., Rouppe van der Voot, L., van Noort, M., & Carlsson, M. 2007a, *ApJ*, 655, 624
- De Pontieu, B., McIntosh, S., Hansteen, V. H., et al. 2007b, *PASJ*, 59, S655
- De Pontieu, B., Title, A. M., Lemen, J. R., et al. 2014, *SoPh*, 289, 2733
- Hansteen, V. H., De Pontieu, B., Rouppe van der Voot, L., van Noort, M., & Carlsson, M. 2006, *ApJL*, 647, L73
- Heggland, L., Hansten, V., H., De Pontieu, B., & Carlsson, M. 2011, *ApJ*, 743, 142
- Hollweg, J. V., Jackson, S., & Galloway, D. 1982, *SoPh*, 75, 35
- Hollweg, J. V. 1982, *ApJ*, 257, 345
- Iijima, H., & Yokoyama, T. 2017, *ApJ*, 848, 38
- Ji, H., & Daughton, W. 2011, *PhPl*, 18, 1207
- Judge, P. G., & Carlsson, M. 2010, *ApJ*, 719, 469
- Judge, P. G., Reardon, K., & Cauzzi, G. 2012, *ApJ*, 755L, 11
- Kudoh, T. and Shibata, K.: 1999, *ApJ*, 514, 493
- Kumar, P., Karpen, J. T., Antiochos, S. K., Wyper, P. F., DeVore, C. R., & DeForest, C. E. 2019, *ApJ*, 873, 93
- Li, Y., & Ding, M. D. 2017, *ApJ*, 838, 15L
- Lemen, J. R., Title, A. M., & Akin, D. J. et al. 2012, *SoPh*, 275, 17
- Martínez-Sykora, J., Hansten, V., De Pontieu, B., & Carlsson, M. 2009, *ApJ*, 701, 1569
- Martínez-Sykora, J., De Pontieu, B., Hansteen, V. H., et al. 2017, *Science*, 356, 1269
- Matsumoto, T., & Shibata, K. 2010, *ApJ*, 710, 1857
- McGlasson, R. A., Panesar, N. K., Sterling, A. C., & Moore, R. L. 2019, *ApJ*, 882, 16
- Moore, R. L., Tang, F., Bohlin, J. D., & Golub, L. 1977, *ApJ*, 218, 286
- Moore, R. L. 1990, *Mem. Soc. Astron. Ital.*, 61, 317
- Moreno-Insertis, F., Galsgaard, K., & Ugarte-Urra, I. 2008, *ApJ*, 673, 211
- Morita, S., Shibata, K., UeNo, S., Ichimoto, K., Kitai, R., & Otsuji, K. 2010, *PASJ*, 62, 901
- Morton, R. J., Srivastava, A. K., & Erdélyi, R. 2012, *A&A*, 542, A70
- Nishizuka, N., Shimizu, M., Nakamura, T., Otsuji, K., Okamoto, T. J., Katsukawa, Y., & Shibata, K. 2008, *ApJ*, 683L, 83
- Nishizuka, N., Nakamura, T., Kawate, T., Singh, K. A. P., & Shibata, K. 2011, *ApJ*, 731, 43
- Panesar, N. K., Sterling, A. C., & Moore, R. L. 2016, *ApJ*, 832L, 7
- Panesar, N. K., Sterling, A. C., & Moore, R. L. 2017, *ApJ*, 844, 131
- Panesar, N. K., Sterling, A. C., & Moore, R. L. 2018, *ApJ*, 853, 189
- Panesar, N. K., Sterling, A. C., & Moore, R. L. 2018, *ApJ*, 868L, 27
- Pariat, E., Antiochos, S. K., & DeVore, C. R. 2009, *ApJ*, 691, 61
- Pereira, T. M. D., De Pontieu, B., & Carlsson, M. 2012, *ApJ*, 759, 18
- Pereira, T. M. D., De Pontieu, B., & Carlsson, M. 2013, *ApJ*, 764, 69
- Rachmeler, L. A. et al. 2019, *SoPh*, submitted, arXiv:1909.05942
- Rouppe van der Voot, L., De Pontieu, B., Hanstten, V. H., Carlsson, M., & van Noort, M. 2007, *ApJL*, 660, L169
- Scherrer, P. H. et al. 2012, *SoPh*, 275, 207
- Shen, Y., Liu, Y., Su, J., & Deng, Y. 2012, *ApJ*, 745, 164
- Shibata, K. 1999, *Ap&SS*, 264, 129
- Shibata, K., & Uchida, Y. 1986, *SoPh*, 103, 299
- Shibata, K., Ishido, Y., Acton, L. W., et al. 1992, *PASJ*, 44, L173
- Shibata, K., Nitta, N., Strong, K. T., Matsumoto, R., Yokoyama, T., Hirayama, T., Hudson, H., & Ogawara, Y. 1994, *ApJ*, 431L, 51

- Shibata, K., Nakamura, T., Matsumoto, T., et al. 2007, *Science*, 318, 1591
- Singh, K. A. P., Isobe, H., Nishizuka, N., Nishida, K., & Shibata, K. 2012, *ApJ*, 759, 33
- Sterling, A. C. 2000 *SoPh*, 196, 79
- Sterling, A. C., & Mariska, J. T. 1990, *ApJ*, 349, 647
- Sterling, A. C., Harra, L. K., & Moore, R. L. 2010, *ApJ*, 722, 1644
- Sterling, A. C., Moore, R. L., & Freeland, S. L. 2011, *ApJ*, 731L, 3
- Sterling, A. C., Moore, R. L., Falconer, D. A., & Adams, M. 2015, *Nature*, 523, 437
- Sterling, A. C., & Moore, R. L., 2016, *ApJL*, 828, 9
- Sterling, A. C., Moore, R. L., Falconer, D. A., Panesar, N. K., & Martinez, F. 2017, *ApJ*, 844, 28
- Suematsu, Y. 1990, in *Progress of Seismology of the Sun and Stars*, ed. Y. Osaki and H. Shibahashi (Berlin: Springer), 211
- Takasao, S., Isobe, H., & Shibata, K. 2013, *PASJ*, 65, 62
- Tsiropoula, G., Tziotziou, K., Kontogiannis, I., Madjarska, M. S., Doyle, J. G., & Suematsu, Y. 2012, *SSR*, 169, 181
- Wyper, P. F., Antiochos, S. K., & DeVore, C. R. 2017, *Nature*, 544, 452
- Yokoyama, T., & Shibata, K. 1995, *Nature*, 375, 42
- Young, P. R., & Muglach, K. 2014, *SoPh*, 289, 3313
- Zhang, Y. Z., Shibata, K., Wang, J. X., et al. 2012, *ApJ*, 750, 16

Table 1. Properties of Hi-C Small-Scale Cool Ejections

Event	x,y location ^a	start ^b	end ^b	lifetime (min) ^c	Type ^d	Width (arcsec) ^e	Height (arcsec) ^e	rise vel (km/s)
1	-79, 249	18:59:54	19:05:21	5.5±0.5	abs smf	6.5	2.0	26 ± 5 ^g
2	-97, 254	18:56:15	19:02:33	6.3±1.0	emit smf	7.0	7.5	27 ± 5 ^g
3	-78, 253	18:58:21	19:04:57	6.6±0.5	surge-like	2.0	6.0	20 ± 4 ^g
4	-69, 252	18:58:45	19:03:45	5.0±0.5	surge-like	2.0	2.0	26 ± 5 ^g
5 ^f	-94, 262	18:52:15	19:02:33	10.3±0.5	surge-like	3.0	9.0	18 ± 4 ^h
6 ^f	-86, 259	18:53:45	18:57:57	4.2±1.0	abs smf	1.5(?)	2.5	24 ± 12 ⁱ
7 ^f	-82, 258	18:53:33	18:58:27	4.9±1.0	surge-like(?)	1.2	3.0	30 ± 15 ⁱ
8	-77, 260	18:57:22	19:02:45	5.4±1.0	abs smf	3.3	2.0	18 ± 4 ^g
9	-75, 264	18:55:21	19:06:45	11.4±1.0	emit smf	3.5	4.0	12 ± 3 ^g
10	-68, 263	18:58:58	19:04:21	5.4±1.0	surge-like	1.5	5.2	29 ± 6 ^g
Averages ^j	—	—	—	6.5±2.4	—	3.2±2.1	4.3±2.5	23±6

^a Based on time of frame in Figure 1(c).

^b From Hi-C when in its observation window, and otherwise from AIA 171. Estimated uncertainties generally ~ 12 –24 s.

^c Estimated uncertainties $\lesssim 1$ m.

^d Description of dominant characteristic morphology. Key: smf=sub-minifilament, abs=absorption, emit=emission.

^e Measured projected against disk. Uncertainties generally $\leq 0.''5$.

^f Rise phase occurred before Hi-C observation window.

^g Rise velocities estimated to be accurate to $\sim 20\%$ when measured with Hi-C.

^h Rise velocity estimated from AIA, but event's large size reduces uncertainty ($\sim 20\%$).

ⁱ Rise velocity estimated from AIA, leading to relatively large uncertainty ($\sim 50\%$).

^j Averages calculated assuming equal weights for all measurements.

Figure 1. (a) Hi-C 2.1 (=“Hi-C”) 172 Å image, showing subregions of the full FOV. The black box is the $40'' \times 40''$ subregion of panels (b), (c), and (d); and red and blue boxes are the respective $20'' \times 20''$ subregions of panels (e) and (f). (b) HMI intensity image, showing a small sunspot and several pores in the FOV. (c) Hi-C 172 Å image in the boxed region of (a). Arrows and labels indicate cool ejection events of Table 1, with each event occurring (approximately) within the accompanying green box. Black boxes indicate the apparent solar-surface footpoint locations for the ejection pointed to by the nearest arrowhead. (d) AIA 171 Å image, with boxes at the same locations as those in (c). Panels (e) and (f) are close-ups (red/blue boxes of (a)), with arrows pointing to (e) events 1 and 3, and (f) events 8 and 9. North is upward and west is to the right in all solar images of this publication. Panels (c), (d), (e), and (f) are available as online animations. Animations (c) and (d) run twice, once with arrows/boxes and once without.

Figure 2. (a) HMI magnetogram of the region shown in Figures 1(b,c,d), with black (white) indicating negative (positive) fields. Overlaid green contours are negative fields at levels of -50 (thin contours), -100 (medium), and -750 (thickest) G. Red contours show positive fields of corresponding levels, with only +50 G levels appearing in this image. Boxes are as in Figure 1(c). (b) Contours of (a) overlaid onto the Hi-C 172 Å image of Figure 1(c). Both panels 2(a) and 2(b) are available as online animations.

Figure 3. *IRIS* SJI 1400 Å images of the Hi-C region of Fig. 1, with black and green arrows and boxes the same as in Fig. 1c. White arrows in (a) and (b) show evolution of a UV feature corresponding to event 5; similarly, in (c) and (d) (with zoomed-in FOV) yellow and turquoise arrows show evolution of UV features corresponding to events 9 and 10. An animation is available.

Figure 4. Number of eruptive events on Sun at a given time as a function of erupting-(mini)filament size, for (left to right) spicules, the Hi-C events of this paper (open red circle), coronal jets, and large-scale erupting filaments. The values for the spicules and the Hi-C features are speculative, since small-scale filaments have not been observed in such jets. The three black circles and the line (which is the best fit to those three points) are the same as in [Sterling & Moore \(2016\)](#). The bottom of the dashed red line is where the Hi-C point would be if we reduced the extrapolated number on the Sun by a factor of ten (consistent with the number of plage cool ejections being overestimated by a factor of ten).

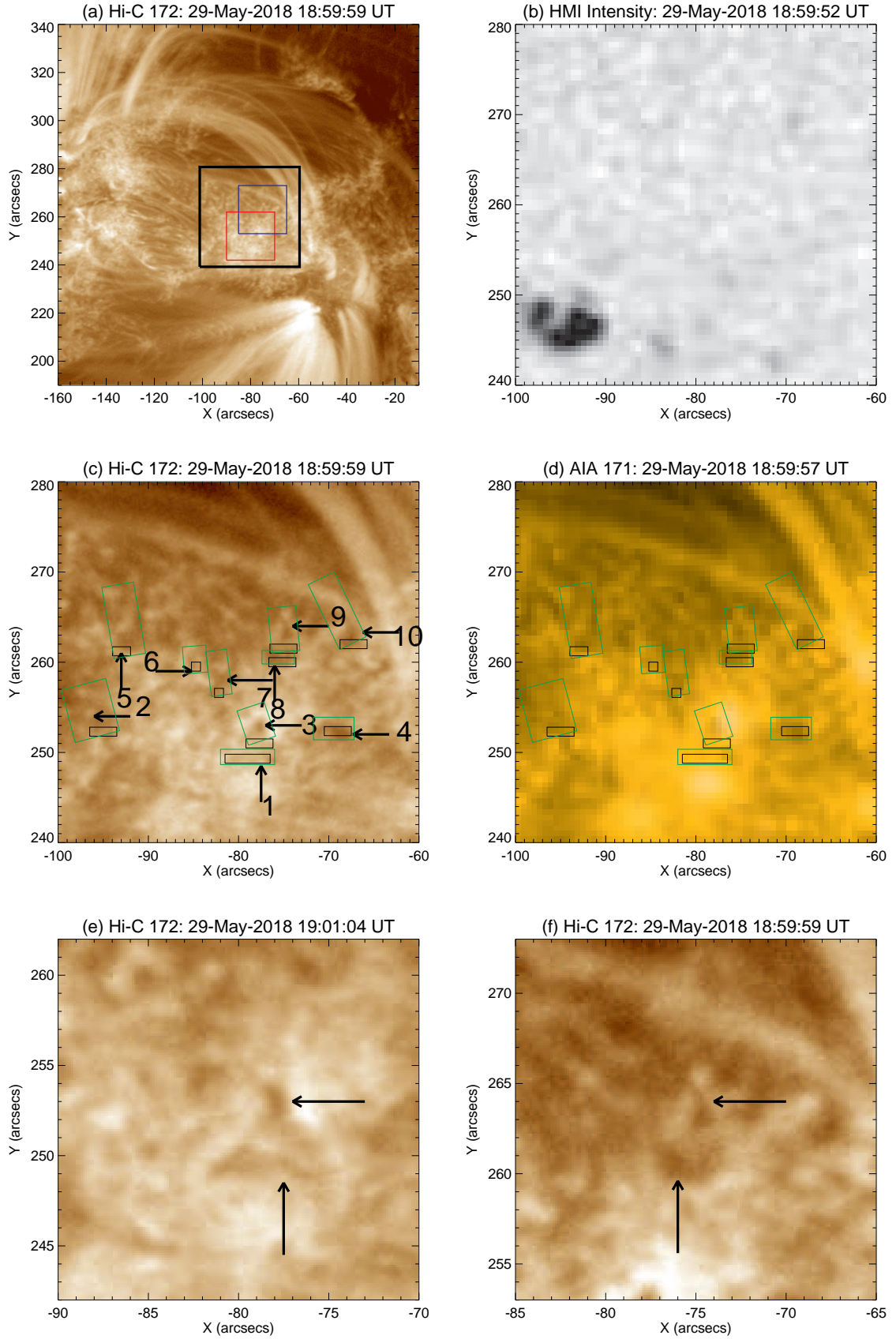


Figure 1

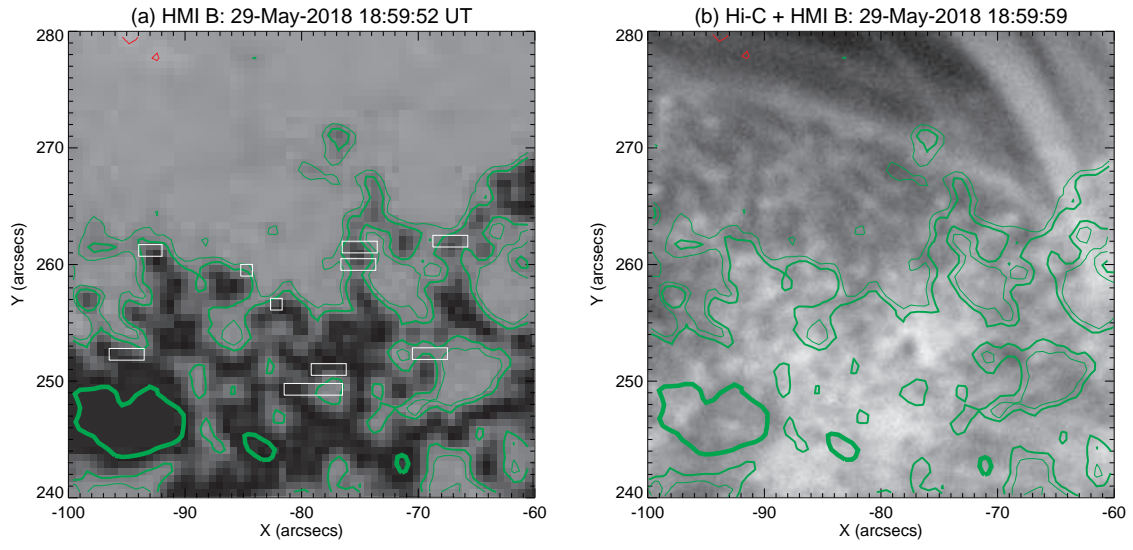


Figure 2

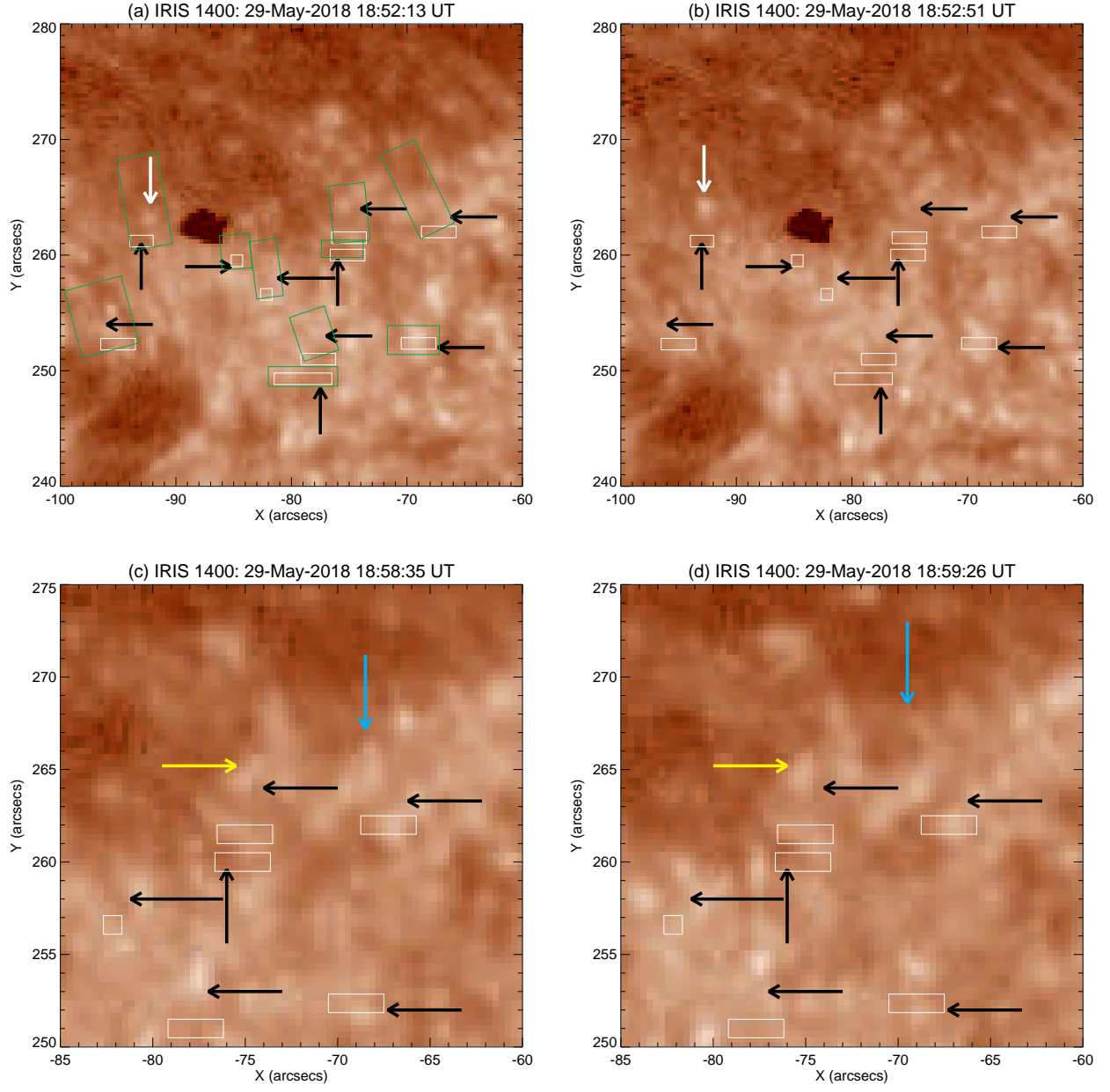


Figure 3

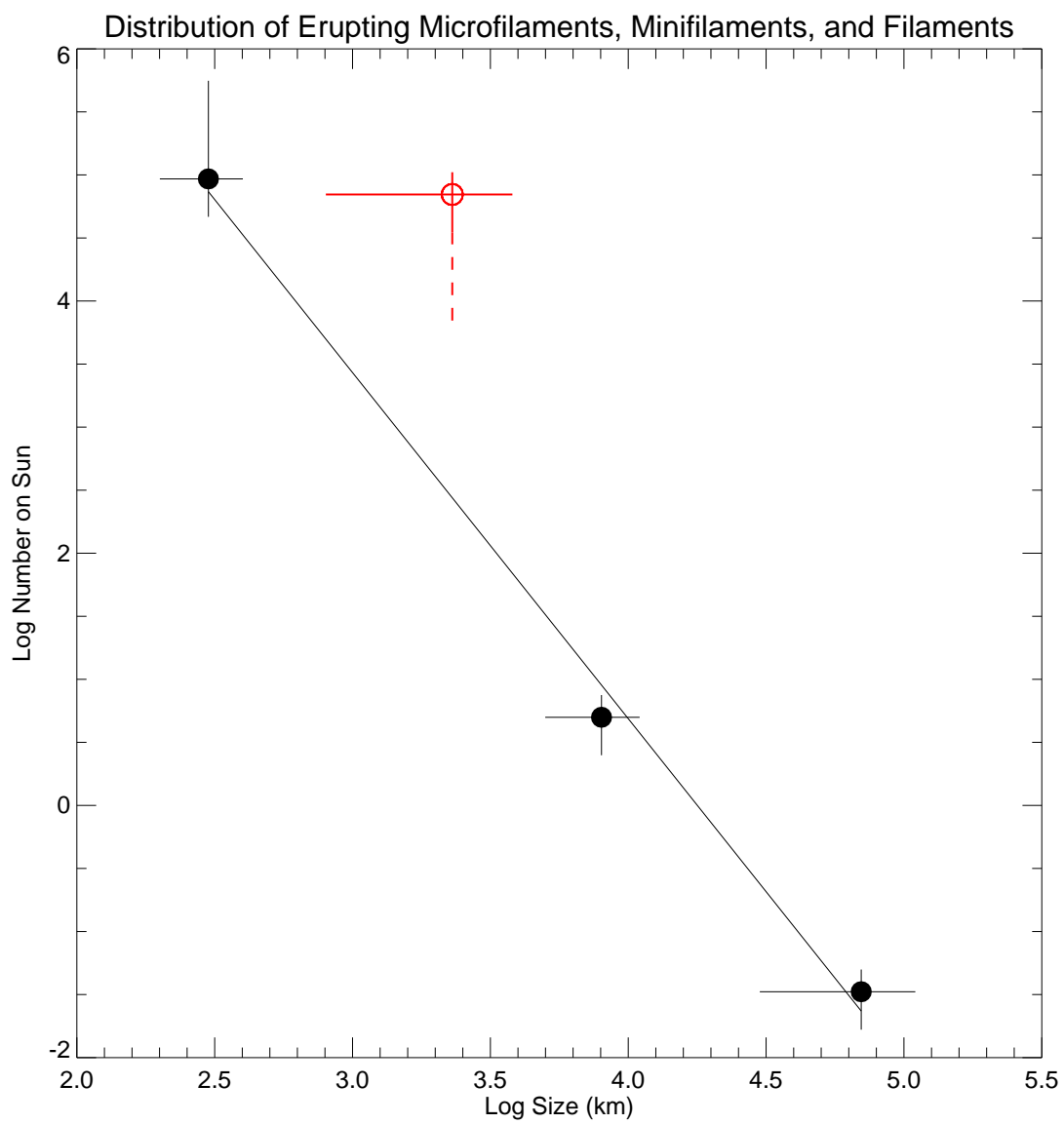


Figure 4